Expanding the absorption bandwidth with two-layer graphene metamaterials in gigahertz frequency range

Ngo Nhu Viet[1,3], Pham Thanh Son[6], Do Khanh Tung[2], Nguyen Hai Anh[2], Do Thuy Chi[4], Nguyen Phon Hai[5], Bui Son Tung[1,2,‡], Bui Xuan Khuyen[1,2], Vu Dinh Lam[1,†]

[1]*Graduate University of Science and Technology, Vietnam Academy of Science and Technology, 18 Hoang Quoc Viet, Cau Giay, Hanoi 100000, Vietnam*

[2]*Institute of Materials Science, Vietnam Academy of Science and Technology, 18 Hoang Quoc Viet, Cau Giay, Hanoi 100000, Vietnam*

[3]*People's Police Academy, Co Nhue 2, Bac Tu Liem, Hanoi, Vietnam*

[4]*Thai Nguyen University of Education, Thai Nguyen 250000, Vietnam*

[5]*Air Defence-Air Force Academy, Kim Son, Son Tay, Ha Noi, Vietnam*

[6]*Faculty of Electronics Engineering, Hanoi University of Industry, Hanoi 11900, Vietnam*

E-mail: [†]lamvd@gust-edu.vast.vn; [‡]tungbs@ims.vast.ac.vn

Received 9 September 2024
Accepted for publication 12 December 2024
Published 25 December 2024

Abstract. *This work investigates the design and performance of a bilayer graphene metamaterial absorber operating in the GHz region. We initially analyzed a single-layer metamaterial absorber composed of a conductive ink graphene structure on a FR-4 dielectric substrate backed by a continuous copper sheet. Subsequently, a second graphene-FR4 layer of identical dimensions was added to create a bilayer structure. While the number of absorption peaks increased, they remained isolated, failing to achieve the desired broadband effect. To overcome this limitation, we explored graphene layers with varying surface resistances. Our findings demonstrate that the bilayer graphene metamaterial absorber achieves an absorption exceeding 90% with a remarkable bandwidth of 9.1 GHz, spanning frequencies from 6.21 GHz to 15.31 GHz. This significant bandwidth expansion is attributed to the synergistic interactions and contributions between the graphene and metal layers within the structure. To gain a deeper understanding of the underlying absorption mechanism, we investigated the surface current distribution, the impact of conductivity, and the individual contributions of each layer. Additionally, we examined the influences of both incident angle and polarization angle on the absorption performance of the proposed*

bilayer metamaterial absorber. These comprehensive analyses provide valuable insights into the mechanisms responsible for the enhanced absorption observed in multilayer metamaterial structures. Our work holds relevance and might be useful to develop electromagnetic wave shielding technologies and devices operating in the GHz frequency range.

Keywords: multilayer; metamaterial absorber; graphene conductive ink.

Classification numbers: 81.05.Xj; 78.67.Pt; 81.05.ue.

1. Introduction

Metamaterials, known for their intriguing properties, are gaining significant attention and finding diverse applications in areas such as negative refractive index [1–5], wireless energy transmission [6–9], and especially, electromagnetic wave absorption [10–15]. One of the most important purposes of metamaterial absorber (MA) is creating the broad absorption bandwidth. With advancements in science, metamaterials can now be fabricated in multilayer configurations to enhance their absorption characteristics [16–20]. Additionally, metamaterials are being developed using combinations of materials such as metal-dielectric, VO_2-dielectric [21], MoS_2-dielectric [22, 23], and graphene-dielectric [24, 25] to optimize their electromagnetic wave absorption properties. Several works have investigated multilayer metamaterial absorbers (MMA) operate in the GHz frequency range with promising results [26, 27]. However, these studies often employ relatively complex structures, with layers varying in size, thickness, or shape, leading to difficulties in the real fabrication. Moreover, these studies do not thoroughly address the interactions between the layers within the MMA structure. In this study, we propose a two-layer structure of broadband absorbing graphene metamaterial. The structure consists of two periodic graphene-dielectric layers placed on a continuous copper metal sheet. The absorption of the multilayer metamaterial exceeds 90%, with an absorption bandwidth reaching 9.1 GHz, covering the frequency range from 6.21 GHz to 15.31 GHz. The study also elucidates the absorption mechanism of the multilayer metamaterial, through investigating the contributions of the structural components and surface current distribution. Due to its symmetrical design, the structure's absorption remains unaffected by different polarization angles. Furthermore, the proposed MA can maintain high absorption even at large incidence angles. It has potential applications in electromagnetic wave shielding, energy harvesting, and self-powered sensors... [28, 29]

2. Multilayer metamaterial structure and methods

Table 1. Metamaterial design parameters.

a	b	c	t_d	t_m	t_g
10 mm	8 mm	1.5 mm	1.7 mmm	0.035 mm	0.1 mm

The metamaterial structure diagram is shown in Fig. 1a. The single-layer graphene structure consists of a plus-shaped graphene layer with length b, width c and thickness t_g and a FR-4 dielectric layer with thickness t_d placed on a continuous copper metal plate of thickness t_m in Fig. 1a. The unit cell size is a, FR-4 is used with dielectric constant $\varepsilon = 4.3$ and loss tangent of 0.025.
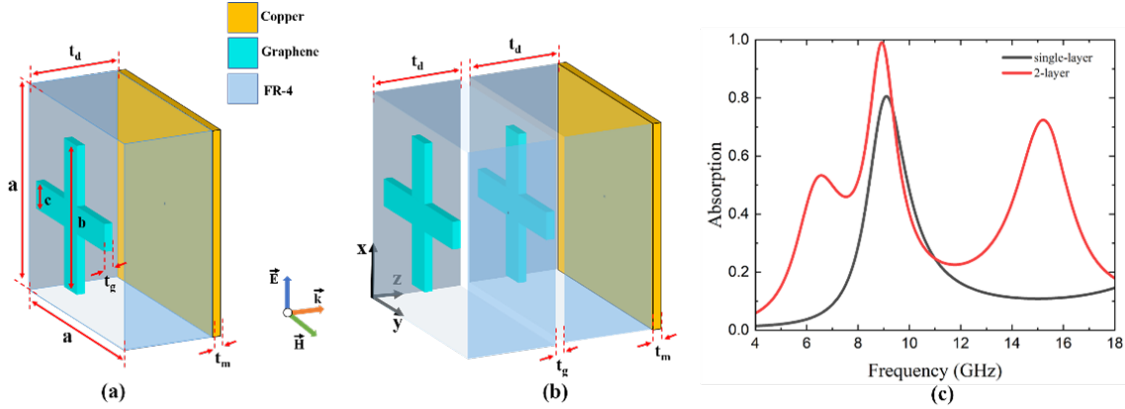
Fig. 1. Proposed metamaterial structure (a) single-layer graphene, (b) 2-layer graphene and absorption spectra of single-layer and 2-layers graphene (2 Ω/sq) with dielectric layer thickness t_d=1.7 mm (c).

The electrical conductivity of copper is 5.96×10^7 S/m, while graphene conductive ink has a surface resistance of 80 Ω/sq. Fig. 1b depicts a 2-layer graphene metamaterial structure, in which 2 layers of graphene-FR-4 have the same size and resemble a single-layer metamaterial structure placed on a continuous copper metal sheet. The values of the constructs are shown in Table 1. To broaden the absorption bandwidth, numerous studies have employed multilayer metamaterial structures. However, these designs often involve complex, multi-layered configurations with varying layer sizes, making fabrication challenging. Building upon these studies and leveraging the properties of graphene, we propose a 2-layer metamaterial structure that offers several advantages: simplified fabrication, optimal thickness, and high absorption efficiency across a wide bandwidth. Due to the identical design of the two structural metamaterial layers, the possible fabrication process in reality is relatively simple. Each layer might be produced by inkjet or screen printing graphene conductive ink onto an FR-4 dielectric substrate. The layers are subsequently bonded together using a specialized silicone adhesive that does not compromise the absorption capabilities of the structure.

In this research, multilayer metamaterial absorbers (MMA) was designed for simulating and analyzing their electromagnetic properties utilizing CST Microwave Studio software. The interaction between electromagnetic waves and materials is described by Maxwell's equations, which are solved by employing the finite integration technique. During simulation, a plane wave with a wave vector, *k*, perpendicular to the MA surface and the E-H plane parallel to the structure surface is considered. Periodic boundary conditions are enforced for the unit cells along the *x* and *y* axes (E-H plane), while the structure is open in the *z* direction. Key simulation results encompass reflection parameters (S_{11}) and transmission parameters (S_{21}). Additionally, the absorption of the MA, denoted as A(Ω), is computed using the formula:

$$A(\Omega) = 1 - R(\Omega) - T(\Omega), \tag{1}$$

where $R(\Omega) = |S_{11}|^2$ is reflection and $T(\Omega) = |S_{21}|^2$ is transmission.

3. Results and discussion

Figure 1c shows the absorption spectra of single-layer and double-layer graphene (2 Ω/sq) metamaterials with a dielectric layer thickness of $t_d = 1.7$ mm. The single-layer graphene metamaterial exhibits one absorption peak at 9.1 GHz with a relatively low absorption of 80.55%. When the number of layers is increased to two, the number of absorption peaks increases to three within the 4-18 GHz range. These peaks occur at frequencies of 6.57 GHz, 8.92 GHz, and 15.21 GHz, with corresponding absorption intensities of 52.51%, 99.13%, and 72.41%. This indicates that increasing the number of layers in the metamaterial structure creates additional absorption peaks, which may result from the interaction between the layers.
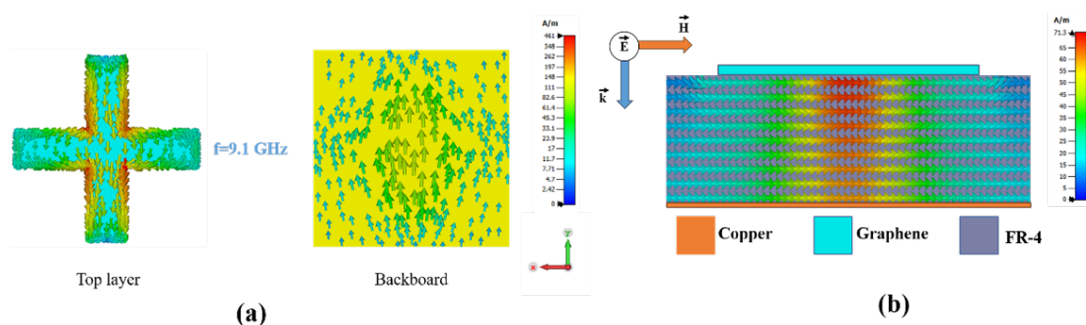

Fig. 2. Surface current distribution (a) and magnetic field distribution (b) of metamaterial graphene (2 Ω/sq) monolayer with dielectric layer thickness $t_d = 1.7$mm at 9.1GHz.

To clarify the absorption behavior, the surface current distribution of the structure was investigated. The surface current distribution of the single-layer metamaterial structure is shown in Fig. 2a. The results show that the surface current of the upper resonant layer flows parallel and opposite to the surface current of the bottom continuous metal layer. Therefore, at the frequency of 9.1 GHz, magnetic resonance appears due to the interaction between the patterned layer and the bottom continuous metal layer. To confirm this, the magnetic field distribution of the structure was also calculated and is depicted in Fig. 2b. The magnetic field moves parallel in the dielectric layer, indicating the presence of magnetic resonance in this case.

Figure 3a presents the surface current distribution of the two-layer graphene (2 Ω/sq) metamaterial with a dielectric layer thickness $t_d = 1.7$ mm at the first resonance frequency $f = 6.57$ GHz. At the frequency of 6.57 GHz, the two upper patterned layers have parallel currents running in the same direction, while the middle patterned layer and the bottom continuous metal layer have parallel surface currents running in opposite directions. Therefore, the absorption peak at this frequency is due to the electrical interaction between the two upper layers and the magnetic interaction between the two lower layers of the structure. To further clarify, the magnetic field distribution is also investigated and shown in Fig. 3b. Only in the lower dielectric layer, the magnetic field forms parallel lines with strong intensity, indicating that magnetic resonance has occurred at this location.

The second absorption peak of the structure corresponds to the frequency of 8.92 GHz. As shown in Fig. 4a, the surface currents between the two upper layers and the surface currents between the two bottom layers tend to run in opposite directions. This indicates that magnetic
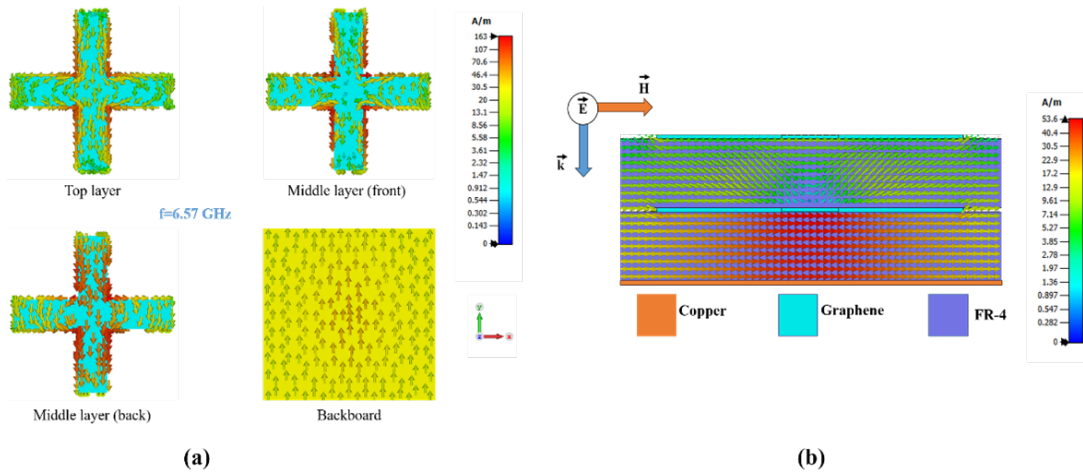
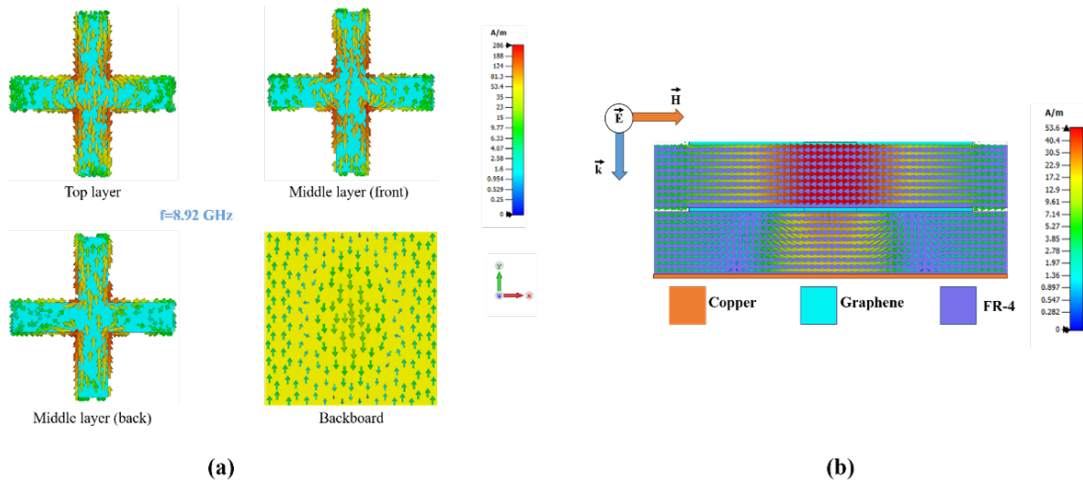**Fig. 3.** Surface current distribution (a) and magnetic field distribution (b) of 2-layers graphene (2 Ω/sq) metamaterial with dielectric layer thickness t_d = 1.7 mm at f_1 = 6.57 GHz.

Fig. 4. Surface current distribution (a) and magnetic field distribution (b) of 2-layers graphene (2 Ω/sq) metamaterial with dielectric layer thickness t_d = 1.7 mm at f_2 = 8.92 GHz.

resonance between adjacent layers is the cause of the absorption peak at 8.92 GHz. To be more clarified, the magnetic field distribution of the structure at this frequency is simulated, as shown in Fig. 4b. A clear magnetic resonance can be seen in the upper dielectric layer when the magnetic field is strong and forms parallel lines in the same direction. In the lower dielectric layer, at the position corresponding to the plus sign structure, magnetic resonance also appears, forming parallel lines. However, outside that position, the magnetic field changes direction. This effect is also observable in the bottom continuous metal plate surface current, as shown in Fig. 4a.
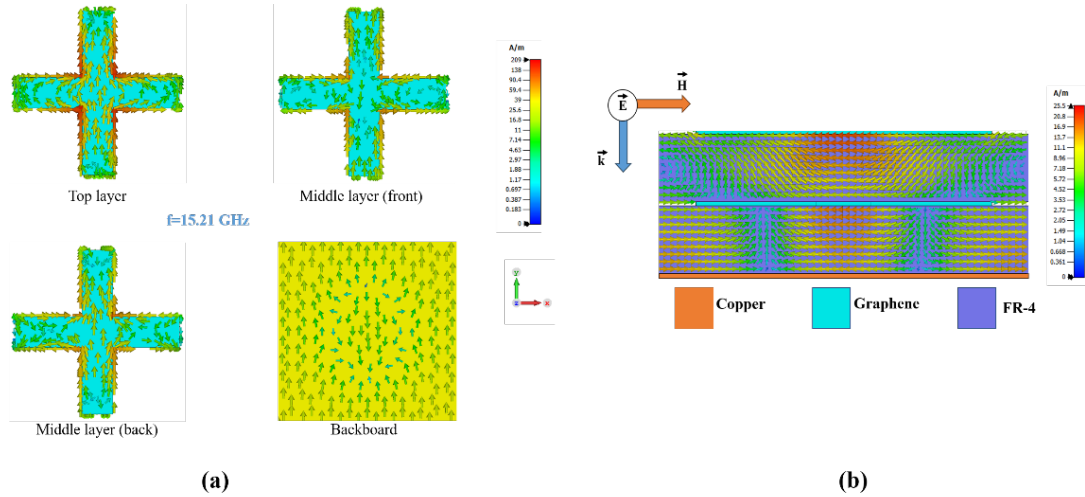
Fig. 5. Surface current distribution (a) and magnetic field distribution (b) of 2-layers graphene (2 Ω/sq) metamaterial with dielectric layer thickness t_d = 1.7 mm at f_3 = 15.21 GHz.

Figure 5a shows the surface current distribution at the third resonance frequency of 15.21 GHz for the two-layer graphene structure (2 Ω/sq) with a dielectric thickness of t_d =1.7 mm. Resonance occurs in the two upper layers, where the upper layers exhibit electric resonance due to the surface currents flowing in the same direction and parallel to each other. In the two bottom layers, the currents flow in anti-parallel directions at the plus sign position. However, on the continuous metal sheet, a high-intensity current appears at a position outside the plus sign, flowing in the same direction as the surface current of the middle layer of graphene. Therefore, both electric and magnetic resonances are present here. This is also demonstrated by the magnetic field distribution shown in Fig. 5b. Due to electric resonance, the magnetic field in the upper dielectric layer flows in a vortex. In the lower dielectric layer, magnetic resonance occurs clearly at the plus sign position, but at adjacent positions, the magnetic field is affected and changes direction. This observation is consistent with the surface current distribution on the continuous metal plate shown in Fig. 5a.

When the number of layers in the metamaterial structure increases, the number of absorption peaks also increases, but broadband absorption is not observed. Therefore, the variation in the square resistance of graphene is examined. In Fig. 6a, when the graphene surface resistance is 2 Ω/sq, the absorption spectrum exhibits three distinct peaks at 6.81 GHz, 9.01 GHz, and 15.59 GHz. As the graphene surface resistance increases, the first and third peaks intensify, while the second peak weakens and the overall absorption background strengthens. At a surface resistance of 50 Ω/sq, the second peak becomes indistinguishable from the background. When the surface resistance reaches 80 Ω/sq, the bilayer graphene metamaterial structure achieves an absorption exceeding 90% within the frequency range of 6.21-15.31 GHz, characterized by two prominent peaks at f_1 =7.64 GHz and f_2 =13.54 GHz.

Figure 6b presents the comparison results of the absorption spectra between a 2-layer graphene metamaterial (80 Ω/sq) with a thickness of t_d = 1.7 mm and a single-layer graphene
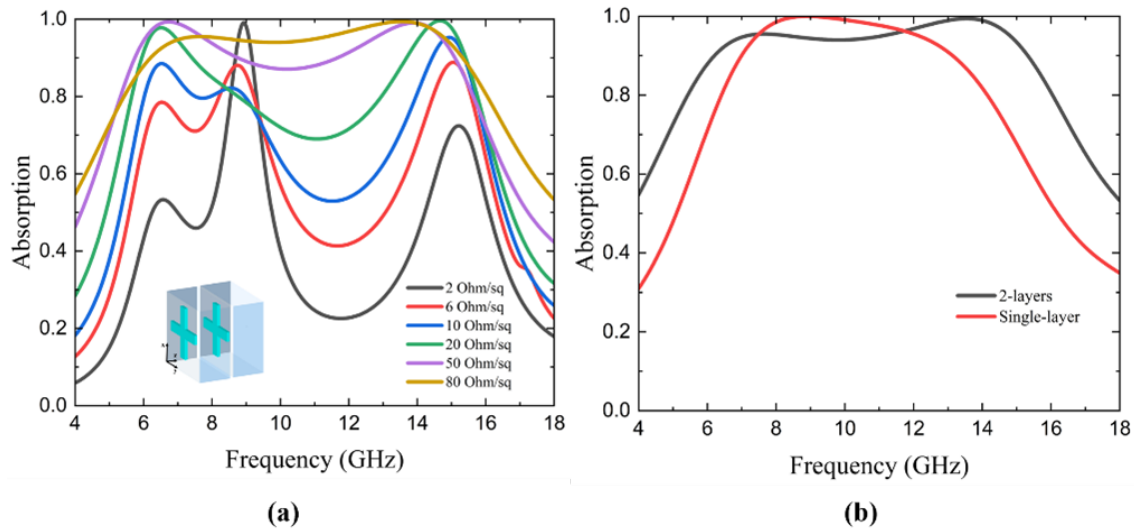
Fig. 6. Absorption spectra of 2-layers of graphene with different resistance (a); Absorption spectrum of 2-layers and single-layer graphene with resistance value of 80 Ω/sq (b).

metamaterial (80 Ω/sq) with a dielectric layer thickness of 3.5 mm, where the total size of both the 2-layer and single-layer metamaterials is the same. The single-layer metamaterial structure exhibits an absorption peak of 99.99% at 8.90 GHz. Despite this high absorption intensity, the structure achieves an absorption bandwidth of only 6.12 GHz with absorption greater than 90%. In contrast, the 2-layer graphene metamaterial demonstrates an absorption bandwidth of 9.1 GHz, representing a 48.69% increase compared to the single-layer structure. The results show that the wide band absorption spectrum of the proposed metamaterial structure is due to two factors, the large surface resistance of the graphene-based ink and the contribution of the 2-layer structure.

Table 2. Comparison of proposed metamaterial structure with some other publications.

Number of layers	Frequency	Bandwidth (>90%)	Manufacturing capacity	Thickness of the sample	References
20	7.8-14.7 GHz	6.9 GHz	Complicated	5.05mm	[30]
29	3.93 – 6.05; 11.64 – 14.55 GHz	2.12 GHz and 2.91 GHz	Complicated	6.3mm	[31]
20	11.39 - 20.46 GHz	9.07 GHz	Complicated	4mm	[32]
2	6.21 -15.31 GHz	9.1 GHz	Simple	3.63mm	This work

Table 2 compares the proposed metamaterial structure with other reported designs. Despite its simplicity with only two layers, the proposed structure demonstrates competitive broadband absorption performance. This advantage is further enhanced by its ease of fabrication, as it relies on a small number of indentical layers of periodic patterns rather than a complex pyramidal geometry with numerous layers.

Figure 7a shows the surface current distribution of a single-layer graphene structure with a dielectric thickness of $t_d = 3.5$ mm and an 80 Ω/sq surface current at 8.9 GHz. It demonstrates that the patterned layer's surface current flows parallel to and in the opposite direction from the bottom metal layer's surface current. The position where the plus sign is located is where the current is mostly concentrated among them. Therefore, the magnetic resonance induced between the bottom continuous metal layer and the graphene layer is responsible for the structure's absorption peak at 8.9 GHz. To validate the magnetic interaction between the two layers, Fig. 7b displays the simulated H-field at 8.9 GHz. The magnetic field distribution in the dielectric layer clearly confirms the excitation of strong magnetic resonance.
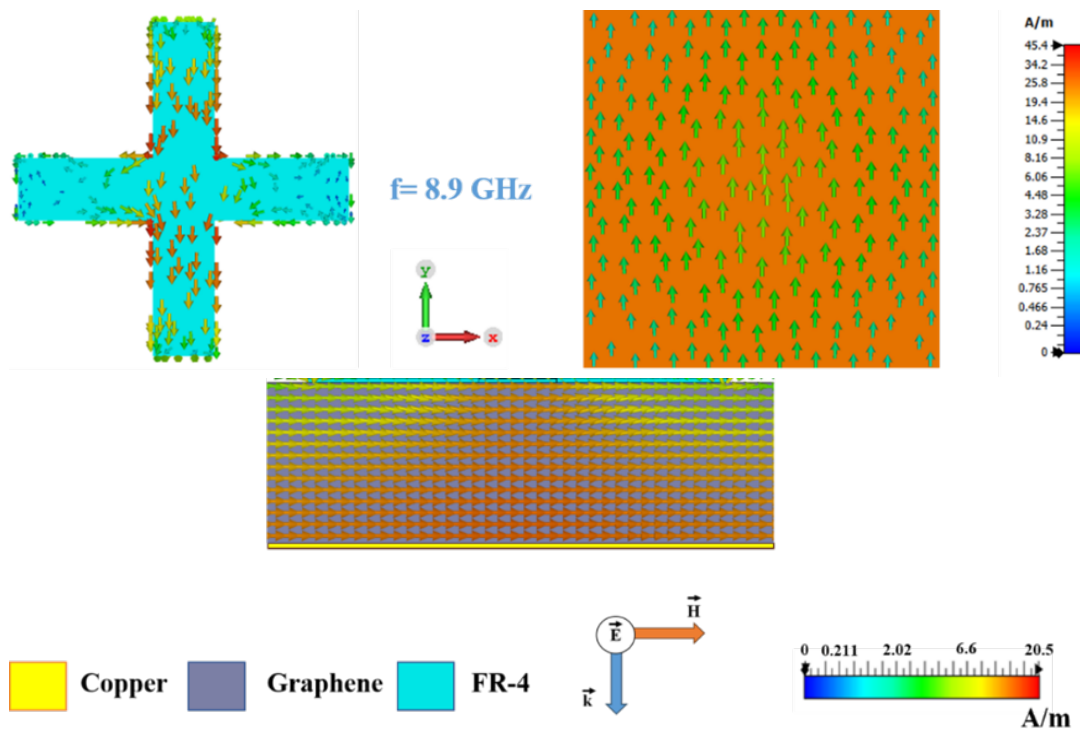

Fig. 7. Surface current distribution (a) and magnetic field distribution of single- layer graphene (80 Ω/sq) metamaterial with dielectric layer thickness $t_d = 3.5$ mm at 8.9 GHz.

The surface current distribution at 7.64 GHz of the two-layer graphene structure is shown in Fig. 8. Due to the two-layer configuration, the interaction between the pairs of layers affects the absorption capacity. In this case, the upper two layers of the metamaterial structure have parallel currents running in the same direction, indicating an electric resonance between these two layers (Figs. 8a,e and 8c,g). However, it is also noticed that there is a phase delay between these two upper layers as depicted in Figs. 8b, 8f and 8d,8h. At intermediate phases of 150° and 330°, the current at the top layer has already reversed direction, while the current at the top surface of the middle layer has not yet. Meanwhile, in the two lower layers of the metamaterial structure, magnetic resonance, which is indicated by anti-parallel currents, is induced as in Figs 8i,n and

8l,p. The surface currents are observed to be strongest at the positions corresponding to the plus sign of the structure. Similar to the above two upper layers, a slight phase delay between the two lower layers are also existed as in Figs. 8k,o and 8m,r. The H-field at 7.64 GHz at phases 0° and 180° of the two-layer structure is shown in Fig. 9. At the plus sign in the upper dielectric layer, the H-field forms a vortex, indicating the occurrence of electric resonance between the two upper layers. In the lower dielectric layer, the H-field moves parallel with its strongest intensity at the plus sign, representing the magnetic resonance between the two lower layers.
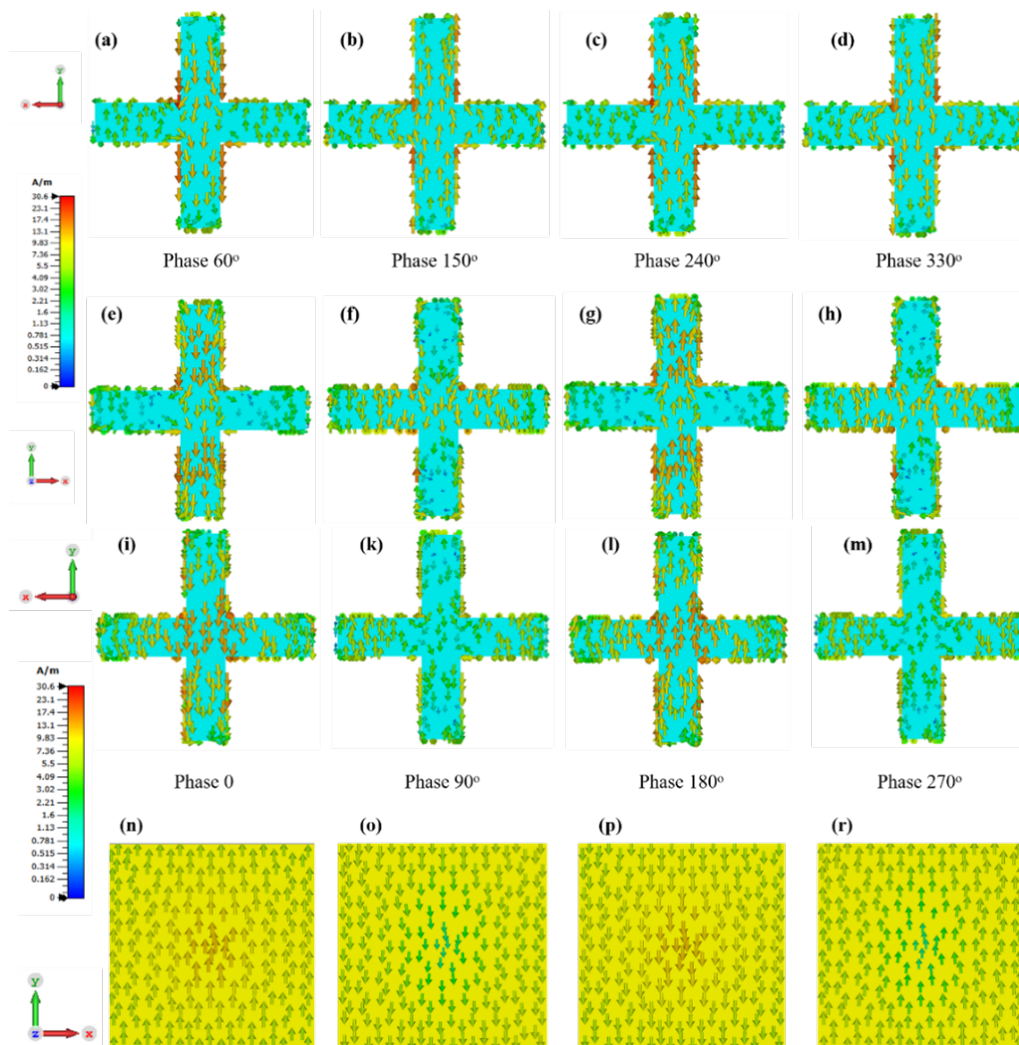

Fig. 8. Surface current distribution of 2-layers graphene (80 Ω/sq) metamaterial with dielectric layer thickness $t_d = 1.7$ mm at $f_1 = 7.64$ GHz; (a)-(d) surface current at the top layer; (e)-(h) upper surface current of the middle layer; (i)-(m) bottom surface current of the middle layer; (n)-(r) surface current of the bottom continuous metal plate.
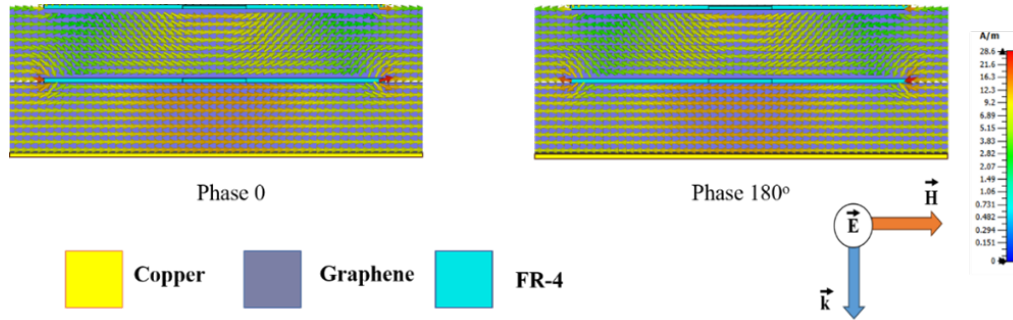
Fig. 9. Magnetic field distribution of 2-layers graphene (80 Ω/sq) metamaterial with dielectric layer thickness t_d = 1.7 mm at f_1 = 7.64 GHz.

Figure 10 displays the surface current distribution of the 2-layer graphene structure (80 Ω/sq) at 13.54 GHz. The surface current distribution for the two upper layers is illustrated in Fig. 10a-h. Panels a-d show the surface current distribution of the top layer at different phases, while panels (e-h) depict the middle layer's surface current distribution at varying phases. The results indicate that the surface currents in these two layers are aligned in the same direction, suggesting the occurrence of electrical resonance. Moreover, no phase delay between the layers is observed.

When examining the surface current distribution of the two lower layers, as shown in Fig. 10i-r, it becomes evident that the currents at positions corresponding to the plus sign in the two layers are in opposite directions, indicative of magnetic resonance. However, the surface current in the continuous metal layer at these positions is weaker and flows in the opposite direction compared to the surrounding areas. This discrepancy might be attributed to the interaction between the layers.

Finally, the influences of the polarization and incident angles on the absorption characteristic are investigated to evaluate the operation of the proposed absorber. The absorption spectrum of the two-layer metamaterial structure with different polarization angles is shown in Fig. 11. Although the polarization angle varies from 0° to 80°, the absorption spectrum remains unchanged. This invariance is due to the symmetrical design of the two-layer metamaterial structure, which ensures that the absorption behavior is unaffected by changes in the polarization angle.

The influence of the incident angle on the absorption of the multilayer metamaterial structure is shown in Fig.12a. The results indicate that broadband absorption is slightly changed for incidence angles θ less than or equal to 40°, while the absorption is reduced more significantly when θ exceeds 40°. Nevertheless, the reduction rates are different at two absorption peaks around 7.64 and 13.54 GHz. The absorption peak at 7.64 GHz drops below 90% at θ = 40° and keeps declining rapidly at the larger incident angle. This decline is attributed to the nature of this absorption frequency, which is based on the magnetic resonance (as shown in Fig.s 8 and 9). Increasing the incident angle weakens the magnetic response of the absorber, resulting in a smaller absorption intensity. At 13.54 GHz, the absorption is less affected by changes in the incident angle with the absorption above 90% up to θ = 70°. Since the absorption peak at this frequency is primarily due to the electric resonance between the layers (as shown in Fig. 10) and the variation of θ in the TE mode does not change the direction of incoming E-field, the electric response of the absorber can maintain quite well the absorption peak at large incident angles.
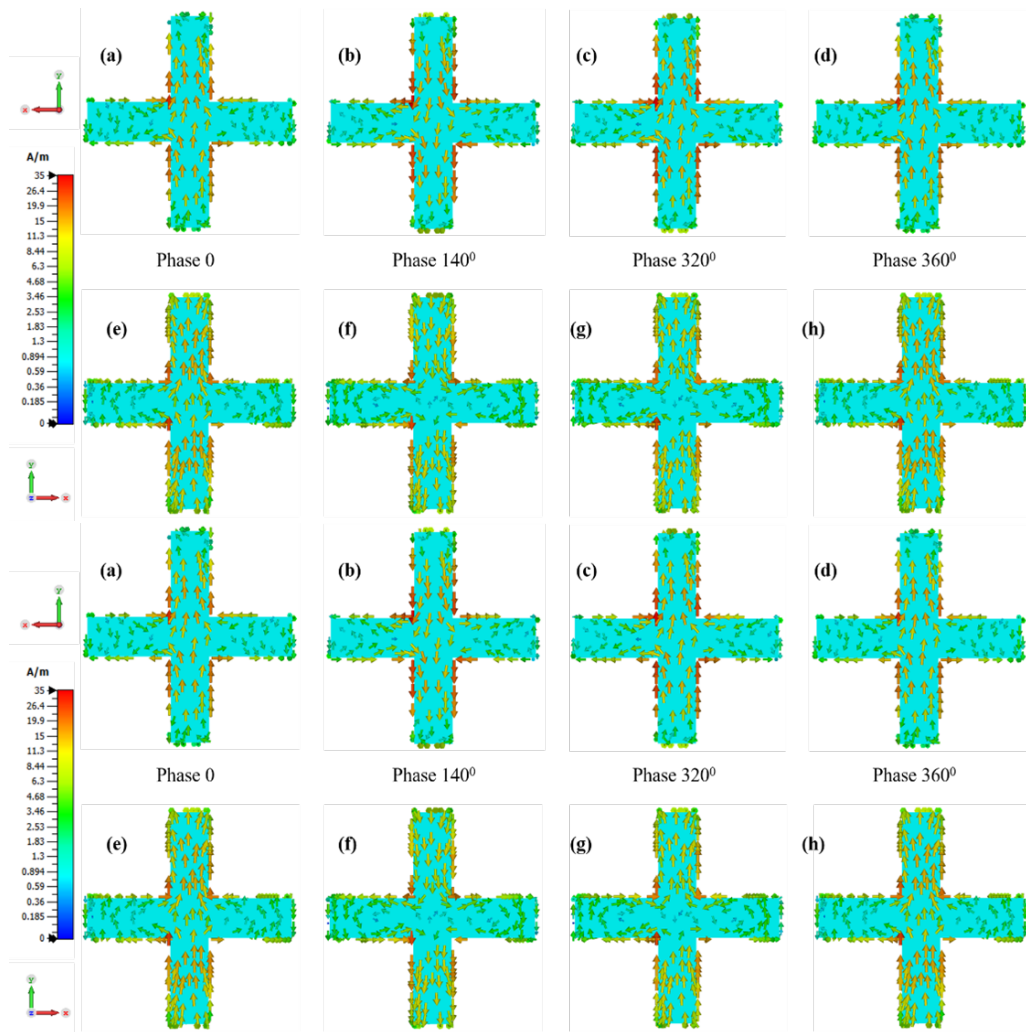
Fig. 10. Surface current distribution of 2-layers graphene (80 Ω/sq) metamaterial with dielectric layer thickness t_d = 1.7 mm at f_2 =13.54 GHz; (a)-(d) surface current at the top layer; (e)-(h) upper surface current of the middle layer; (i)-(m) bottom surface current of the middle layer; (n)-(r) surface current of the bottom continuous metal plate.

The absorption intensity of the 2-layer metamaterial structure in TM mode is shown in Fig. 12b. As the incident angle theta increases gradually from 0 to 40º, the absorption intensity of the entire broadband tends to increase gradually due to changes in impedance matching. When the incident angle theta reaches 60º, the absorption intensity begins to decrease gradually but remains above 90% within the frequency range of 6.72 to 15.66 GHz. Further increasing the incident angle to 70º and 80º causes a sharp drop in the absorption intensity of the 2-layer metamaterial structure to below 90%. The two-layer metamaterial demonstrates a relatively stable absorption at large incident angles. The absorption in TE mode-incidence only maintain quite well around
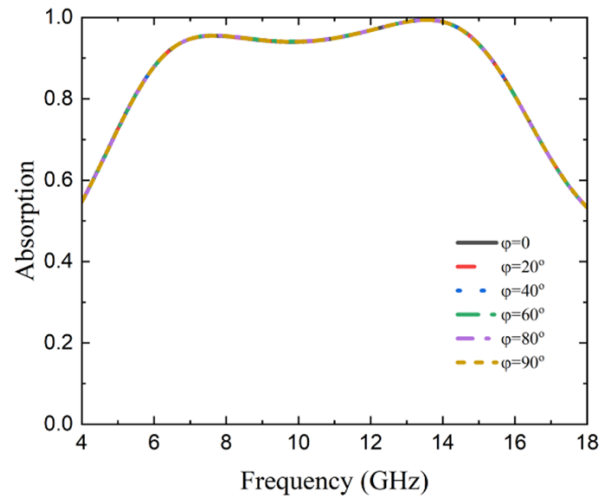
Fig. 11. Effect of polarization angle on absorption intensity of 2-layers graphene structure (80 Ω/sq) with dielectric thickness of 1.7 mm.
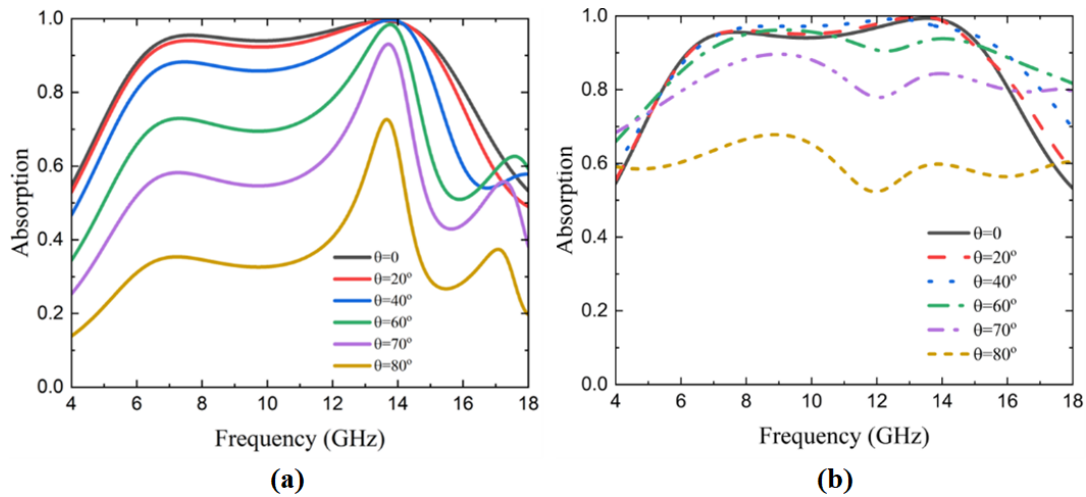

Fig. 12. Absorption intensity of 2-layers graphene metamaterial with different incident angles in TE (a) and TM (b) modes.

a specific frequency, which is more suitable for narrowband applications. On the other hand, the absorption in TM mode-incidence offers enhanced broadband absorption, particularly at larger incident angles. In particular, the structure maintains high absorption for incident angles up to 60 degrees in both polarizations, which is a significant improvement over some recent studies [33,34].

4. Conclusions

We designed and investigated a 2-layered graphene metamaterial that exhibits a broadband absorption in the GHz region. The structure is made up of two resonant layers composed of

graphene pluses stacked on top of two FR-4 dielectric layers, as well as a continuous copper metal sheet at the bottom. The structure has an absorption more than 90% and an absorption bandwidth of 9.1 GHz in the frequency range 6.21-15.31 GHz. By analyzing the distribution of surface current and the role of structural components, the absorption mechanism is elucidated, which relies on both electric and magnetic resonances. Furthermore, because of its symmetrical structure, the structure's absorption performance is unaffected by varied polarization angles, and it also delivers relatively good absorption at varying incidence angles. Our work contributes an efficient approach to create broadband metamaterial absorber by exploiting multi-layer structure, which is useful for applications in communications and electronic devices such as antenna and electromagnetic shielding.

Acknowledgements

Conflicts of Interest

The authors declare no conflict of interest.

References

[1] R. Giri and R. Payal, *Negative-Index Metamaterials*, ch. 10, pp. 205–217. John Wiley & Sons, Ltd, 2023.

[2] P. Mukherjee, S. Banerjee, S. Pahadsingh, W. Bhowmik, B. Appasani and Y. Abdulkarim, *Refractive index sensor based on terahertz epsilon negative metamaterial absorber for cancerous cell detection*, Journal of Optoelectronics and Advanced Materials **25** (2023) 128.

[3] K.-X. Zhang, W.-P. Wu, J.-D. Shao, J. Sun, Q. Yan and J.-Y. Nie, *Substrate-thickness dependence of negative-index metamaterials at optical frequencies*, Appl.Phys. Lett. **124** (2024) 101703.

[4] N. T. Hien, N. X. Ca, B. X. Khuyen, T. Van Huynh, N. S. Khiem, N. T. Tung *et al.*, *Active control of the hybridization effect of near-field coupled resonators in metamaterial for a tunable negative refractive index at terahertz frequencies*, J. Phys. Chem. Sol. **156** (2021) 110173.

[5] H. A. Nguyen, B. S. Tung, X. C. Nguyen, V. D. Lam, T. H. Nguyen and B. X. Khuyen, *Tunable dynamic metamaterial for negative refraction*, J. Phys. Chem. Sol. **186** (2024) 111804.

[6] U. K. Mudhigollam and M. R. Mandava, *An analytical study of wireless power transmission system with metamaterials*, Energy Harvest. Syst. **11** (2024) 20220135.

[7] M. Wang, J. Guo, Y. Shi, M. Wang, G. Song and R. Yin, *A metamaterial-incorporated wireless power transmission system for efficiency enhancement*, Int. J. Circuit Theory Appl. **51** (2023) 3051.

[8] W. C. Harris and D. S. Ricketts, *Maximum gain enhancement in wireless power transfer using anisotropic metamaterials*, Sci. Rep. **13** (2023) 7726.

[9] W. Adepoju, I. Bhattacharya, M. Sanyaolu, M. B. Enagi, E. N. Esfahani, T. Banik *et al.*, *Metaheuristic-based optimization and prototype investigation of low frequency metamaterial for wireless power transfer application*, IEEE Access **11** (2023) 54577.

[10] K. V. Babu and G. N. J. Sree, *Design and circuit analysis approach of graphene-based compact metamaterial-absorber for terahertz range applications*, Opt. Quantum Electron. **55** (2023) 769.

[11] B.-X. Wang, G. Duan, C. Xu, J. Jiang, W. Xu and F. Pi, *Design of multiple-frequency-band terahertz metamaterial absorbers with adjustable absorption peaks using toothed resonator*, Mater. Des. **225** (2023) 111586.

[12] Y. Liu, W.-Z. Ma, Y.-C. Wu, D. Meng, C. Dou, Y.-Y. Cheng *et al.*, *A metamaterial absorber with a multi-layer metal–dielectric grating structure from visible to near-infrared*, Opt. Commun. **542** (2023) 129588.

[13] D. Pham-Van, C. Tran-Manh, N. Bui-Huu, A. Pham-Phuong, A. Ta-Minh-Tuan, D. Pham-Hoang *et al.*, *Broadband microwave coding absorber using genetic algorithm*, Opt. Mater. **147** (2024) 114679.

[14] T. K. T. Nguyen, T. M. Nguyen, H. Q. Nguyen, T. M. T. Nguyen, T. H. T. Ho, T. M. Pham *et al.*, *A simple design of water-based broadband metamaterial absorber for thz applications*, Comm. Phys. **33** (2023) 93.

[15] B. X. Khuyen, N. Van Ngoc, D. N. Dung, N. P. Hai, N. T. Tung, B. S. Tung *et al.*, *Dual-band infrared metamaterial perfect absorber for narrow-band thermal emitters*, Journal of Physics D: Applied Physics **57** (2024) 285501.

[16] G. Peng, P.-X. Ke, L.-C. Tseng, C.-F. Yang and H.-C. Chen, *The design of a multilayer and planar metamaterial with the multi-functions of a high-absorptivity and ultra-broadband absorber and a narrowband sensor*, Photonics **10** (2023) 804.

[17] H. W. Lan, Z. M. Li, X. L. Weng, L. Qi, K. Li, Z. R. Zhou *et al.*, *Low-frequency broadband multilayer microwave metamaterial absorber based on resistive frequency selective surfaces*, Appl. Opt. **62** (2023) 1096.

[18] B. X. Khuyen, N. N. Viet, P. T. Son, B. H. Nguyen, N. H. Anh, D. T. Chi *et al.*, *Multi-layered metamaterial absorber: Electromagnetic and thermal characterization*, Photonics **11** (2024) 219.

[19] G. Ma, X. Li, F. Hu, T. Deng, L. Li, C. Gao *et al.*, *A novel multilayer broadband terahertz metamaterial absorber based on three-dimensional printing and microfluidics technologies*, IEEE Trans. Terahertz Sci. Technol. (2024) .

[20] P. Sun, H. Feng, L. Su, S. Nie, X. Li, Y. Zhou *et al.*, *Metamaterial ultra-wideband solar absorbers based on a multi-layer structure with cross etching*, Phys. Chem. Chem. Phys. **25** (2023) 10136.

[21] Y. Lian, Y. Li, Y. Lou, Z. Liu, C. Jiang, Z. Hu *et al.*, *Adjustable trifunctional mid-infrared metamaterial absorber based on phase transition material VO_2*, Nanomaterials **13** (2023) 1829.

[22] D. T. Ha, M. H. Nam, B. S. Tung, B. X. Khuyen, V. D. Lam and Q. Le-Van, *Ultra-broadband and flexible metamaterial absorber based on mos2 cuboids with mie resonances*, J. Korean Phys. Soc. **82** (2023) 1047.

[23] F. Cai and Z. Kou, *A novel triple-band terahertz metamaterial absorber using a stacked structure of mos2 and graphene*, Photonics **10** (2023) 643.

[24] R. Zheng, Y. Liu, L. Ling, Z. Sheng, Z. Yi, Q. Song *et al.*, *Ultra wideband tunable terahertz metamaterial absorber based on single-layer graphene strip*, Diamond and Related Materials **141** (2024) 110713.

[25] A. Didari-Bader and H. Saghaei, *Penrose tiling-inspired graphene-covered multiband terahertz metamaterial absorbers*, Opt. Express **31** (2023) 12653.

[26] A. Verma, N. Narang, D. Singh and G. Varma, *An experiment with electronic waste for improving the performance of fsss embedded multilayer microwave absorber*, J. Mater. Sci.: Mater. Electron. **34** (2023) 737.

[27] F. Ding, Y. Cui, X. Ge, Y. Jin and S. He, *Ultra-broadband microwave metamaterial absorber*, Appl. Phys. Lett. **100** (2012) .

[28] M. Bağmancı, L. Wang, C. Sabah, M. Karaaslan, L. C. Paul, T. Rani *et al.*, *Broadband multi-layered stepped cone shaped metamaterial absorber for energy harvesting and stealth applications*, Eng. Rep. **6** (2024) e12903.

[29] M. M. Hasan, M. Moniruzzaman, P. Kirawanich, T. Alam, I. B. Yahya, A. M. Alrashdi *et al.*, *Frequency and bandwidth modulation of a wide band-stop metamaterial for emi shielding applications*, Opt. Laser Technol. **172** (2024) 110515.

[30] L. Du, T. Shi, S. Dong, X. Wang, M. Zhou, J. Zhao *et al.*, *Ultra broadband microwave metamaterial absorber with multiple strong absorption peaks induced by sandwiched water resonators*, Appl. Phys. A **128** (2022) 864.

[31] Y. J. Kim, Y. J. Yoo, K. W. Kim, J. Y. Rhee, Y. H. Kim and Y. Lee, *Dual broadband metamaterial absorber*, Opt. Express **23** (2015) 3861.

[32] G. Deng, H. Sun, K. Lv, J. Yang, Z. Yin, Y. Li *et al.*, *Enhanced broadband absorption with a twisted multilayer metal–dielectric stacking metamaterial*, Nanoscale Adv. **3** (2021) 4804.

[33] A. Armghan, K. Aliqab and M. Alsharari, *Polarization and wide-angle incidence mxene-based metamaterial absorber for visible and infrared wavelengths*, Opt. Quantum Electron. **56** (2024) 1265.

[34] X. Huang, M. Cao, D. Wang, X. Li, J. Fan and X. Li, *Broadband polarization-insensitive and oblique-incidence terahertz metamaterial absorber with multi-layered graphene*, Opt. Mater. Express **12** (2022) 811.